Sādhanā Vol. 28, Parts 3 & 4, June/August 2003, pp. 799–814. © Printed in India

In-situ studies on phase transformations under electron irradiation in a high voltage electron microscope

S BANERJEE

Materials Science Division, Bhabha Atomic Research Centre, Mumbai, India
e-mail: sbanerji@magnum.barc.ernet.in

Abstract. High voltage electron microscopy (HVEM), using electron energies adequate for causing displacements of atoms from lattice sites, is a very effective technique for studying mechanisms of solid state phase transformations and for charting the path of phase evolution in real time. This has been demonstrated in studies on chemical ordering in nickel–molybdenum alloys and on the $\beta \rightarrow \omega$ displacement ordering in zirconium–niobium alloys. The enhanced diffusivity due to electron irradiation makes it possible to explore a sequence of phase evolution at low enough temperatures where even some first-order transformations are driven by free energy (G) instabilities with respect to the relevant order parameter (η). Specific issues addressed in these studies are reviewed in this paper.

Keywords. Electron irradiation; phase transformations; chemical ordering; displacement ordering; electron microscopy.

1. Introduction

Radiation-induced defects are known to play a major role in influencing phase transformations in several alloy systems. Studies on this subject have attracted renewed interest as can be seen from several publications (Schulson 1979; Russell 1984). Random displacement of atoms and replacement collision sequences resulting from radiation damage are responsible for production of anti-site defects in chemically ordered structures. This point was experimentally established by demonstrating that an ordered arrangement of atoms could be completely destroyed by radiation damage (Penission & Bourret 1975). The opposite process, i.e. the restoration of order, can also be aided by point defects created by radiation at temperatures where the mobility of vacancies become quite significant. The fact that the order–disorder transformation can be induced in either direction in an alloy system by suitably altering the displacement rate and the temperature has been established in some studies (Banerjee *et al* 1984). High Voltage Electron Microscopy (HVEM) has proved to be a very effective technique in studying the real time progress of the *order* $\leftrightarrows$ *disorder* transition under irradiation.

The issue of continuous versus discrete transformations is of fundamental interest in phase transformations research. However, there are only a few alloy systems in which competition between continuous and discrete transformations can be studied. The interest in the ordering reactions in the Ni–Mo system is essentially due to the fact that several competing ordering reactions, including a second-order transition, are present. The interplay of different ordering

processes and of the instabilities/metastabilities associated with them can be studied over a wide temperature range in situ in an HVEM. Radiation-enhanced diffusion in such experiments allows one to explore the evolution of the ordering process at temperatures lower than the relevant instability temperatures. The nature of the short range order (SRO) in the Ni–Mo system has been studied extensively and different structural models have emerged from these studies (Das & Thomas 1974; Banerjee 1989). HVEM results, as will be discussed in later sections, have been able to show that these models are not contradictory but are different descriptions of the same physical reality.

A continuous ordering transformation can be visualized as a continuous amplification of a concentration wave of short wavelength with an appropirate wave vector which corresponds to the ordered structure. Progressive changes in the diffuse intensity patterns during the early stages of ordering in an HVEM provides an insight into the "structure" of the evolutionary stages of ordering. In fact, recent Monte Carlo simulation (Hata *et al* 1998) has also validated some of the conclusions arrived at earlier from the diffuse intensity patterns recorded in HVEM experiments (Banerjee *et al* 1984).

The displacive $\beta \rightarrow \omega$ transformation is known to exhibit diffuse intensity distribution prior to the formation of the "perfect" ω structure. Real-time evolution of the ω structure under 1 MeV electron irradiation at 300 K has been recorded in HVEM experiments. The similarity of the diffuse intensity distribution in these two cases brings out the importance of the lattice collapse mechanism in both the cases.

2. Crystallography of the ordered phases in Ni–Mo system

The equilibrium phase diagram of the Ni–Mo system shows three ordered phases: Nl_4Mo, Ni_3Mo and δ-NiMo (van Tendeloo 1976). In addition a metastable Ni_2Mo phase has been encountered in this system.

The equilibrium Ni_4Mo phase ($D1_a$ structure), which has an order–disorder transition temperature of 1140 K, has a body-centred tetragonal structure with the following lattice parameters:

$$a_1 = a_2 = 5{\cdot}725\text{Å}, a_3 = 3{\cdot}566\text{Å}.$$

The unit cell of this structure and the lattice correspondence between the $D1_a$ and the corresponding disordered fcc structure is shown in figure 1a.

The equilibrium Ni_3Mo phase has an orthorhombic structure with the following lattice parameters:

$$a_1 = 5{\cdot}064\text{Å}; a_2 = 4{\cdot}224\text{Å}; a_3 = 4{\cdot}48\text{Å}.$$

This equilibrium structure is not coherent with the disordered fcc structure and does not appear in the initial stages of ordering of alloys having compositions in the vicinity of Ni_3Mo.

A metasable Ni_3Mo phase with DO_{22} structure which is coherent with fcc has been reported in a number of studies (see for example, van Tendeloo 1976, Martin & Williams, 1984). The equilibrium Ni_3V phase in the Ni–V system which belongs to the $\langle 1\ 1/2\ 0\rangle$ family, has the DO_{22} structure. The relationship between fcc and DO_{22} is shown in figure 1b.

The metastable Ni_2Mo phase has a Pt_2Mo structure, which is body-centred orthorhombic with lattice parameters:

$$a_1 = a_o/\sqrt{2}; a_2 = 3a_o/\sqrt{2}; a_3 = a_o,$$

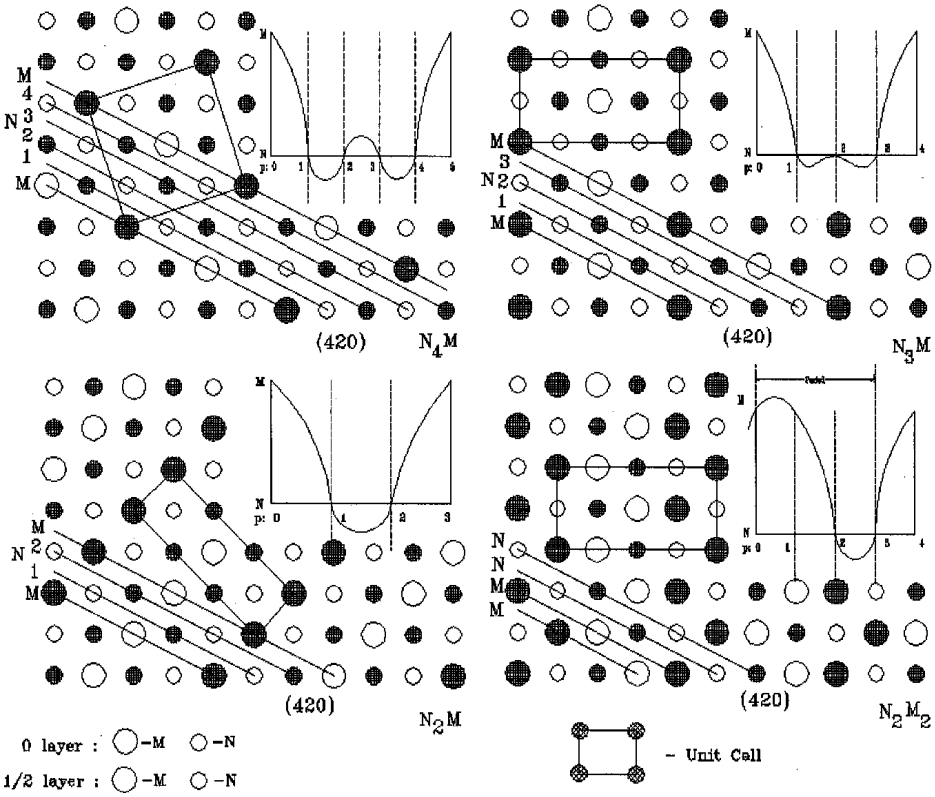

Figure 1. Sequences of Ni layers (N) and Mo layers (4 2 0) planes in **(a)** $Ni_4Mo(D1_a)$, **(b)** $Ni_3V(DO_{22})$, **(c)** metastable Ni_2Mo and **(d)** N_2M_2 structures. Lattice correspondence between the parent *fcc* and the coherent ordered structures are also shown by marking the vectors *ai* and *Ai* corresponding to the unit cells of the former and the latter respectively.

where a_o is the *fcc* lattice parameter. The lattice relationship between Ni_2Mo and *fcc* is shown in figure 1c.

The equilibrium δ-NiMo phase has a complicated structure with space group $P2_12_12_1$. Its structure is orthorhombic but its lattice has a tetragonal symmetry, the lattice parameters being:

$$a_1 = a_2 = 9{\cdot}108\text{Å}; \; a_3 = 8{\cdot}852\text{Å}.$$

The equilibrium $Ni_4Mo(D1_a)$, the metastable $Ni_3Mo(DO_{22})$ and the metastable $Ni_2Mo(Pt_2Mo)$ structures can all be considered superstructures of the disordered *fcc* high temperature phase.

As mentioned earlier, these structures can be described in terms of stacking of {4 2 0} planes that contain either all Ni or all Mo atoms. The Ni_4Mo, Ni_3Mo and Ni_2Mo structures are generated by stacking of all-Mo layers after every 4, 3 and 2 all-Ni {4 2 0} layers respectively. An examination of these structures reveals that each of these structures is associated with a characteristic motif (as indicated by dashed lines) repeated stacking of which results in the generation of these structures. Each of these motifs contains a sub-unit cell cluster which maintains Ni and Mo atoms in the right stoichiometry and can be visualized as a 'molecule' corresponding to each of these intermetallic compounds.

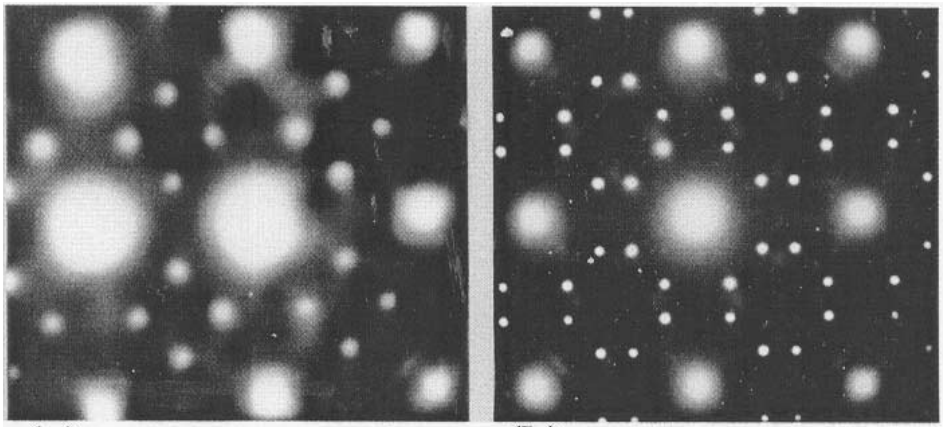

Figure 2. [0 0 1] diffraction pattern from stoichiometric Ni_4Mo alloy: **(a)** SRO; **(b)** LRO

The structure developed by the full amplification of the $\langle 1\ 1/2\ 0\rangle$ concentration wave is depicted in figure 1d. The layering sequence NNMM and the motif characteristic of this structure are also shown in this figure. The similarity of the motifs associated with the N_2M_2 and the $Ni_3Mo(DO_{22})$ structures is to be noted.

The Ni–Mo system is a very good candidate for studying continuous versus discrete transformations for the following reasons.

(a) The short range ordered (SRO) state of alloys in a wide range of composition (8–33% Mo) exhibits diffraction maxima at {1 1/2 0} positions which do not correspond to the superlattice reflections of either the equilibrium or the metastable long range ordered (LRO) structures reported in this system (figure 2).
(b) The competing coherent LRO structures like $Nl_4Mo(D1_a)$, $Ni_3Mo(DO_{22})$, Ni_2Mo (Pt_2Mo type) and the fully amplified {1 1/2 0} concentration wave (designated N_2M_2) which form in this system can all be described in terms of periodic arrays of nickel and molybdenum layers {4 2 0} planes (figure 1). These structures can therefore be generated by introduction and amplification of concentration waves with wave vectors along the $\langle 4\ 2\ 0\rangle$ direction of the reciprocal space. The observation that alloys containing 8–33% Ni quenched from $T > T_c$ shows intensity maxima which do not coincide with superlattice reflections of competing LRO structures raise doubts regarding the nature of the SRO state in these alloys. In the present paper, an attempt is made to narrate how TEM research including that obtained from HVEM studies over about twenty years has progressively elucidated the nature of the SRO structure and the path of the evolution of LRO in these alloys.

3. Structural descriptions of the SRO and the SRO–LRO transitional states

A number of structural descriptions of the SRO state and the transitional states between SRO and LRO have been proposed (Das & Thomas 1974; de Fontaine 1975; de Ridder *et al* 1976; Chevalier & Stobbs 1979; Banerjee *et al* 1984). These descriptions, which have a bearing on the operative mechanisms of the ordering process, cover the full spectrum from the continuous

to the discrete (nucleation and growth) mechanisms. These descriptions are listed in the following in order of their decreasing association with the continuous ordering mechanism and the salient features of each of these are briefly mentioned.

3.1 *Concentration waves*

In order to provide a structural description of an alloy with a short wavelength concentation wave, let us first consider a situation where a single wave with a wavelength appropriate to the evolving superlattice structure extends spatially over a long range. In this case, a single domain of the LRO structure develops in a continuous manner as the wave amplifies. Such a mechanism truly describes a second-order ordering process occurring at the equilibrium transition temperature. This description, however, is purely statistical. The corresponding atomic description requires the formation of atomic clusters of suitable geometries representing motifs of the LRO structure. The amplitude of the wave is directly related to the population density of these clusters, the majority of which remain in phase with the wave. Finally, in the fully ordered structure the structural motifs join in accordance with the superlattice geometry of the LRO structure.

3.2 *Concentration wave packets*

The spatial extension of the concentration wave is visualized to be restricted in this description. Localized wave packets, belonging to several variants of the ordering wave vector remain distributed in space without being related with one another through superlattice translational vectors. An individual wave packet is viewed to be bounded by diffuse interfaces where the wave amplitude gradually tapers off. This description is more appropriate than the former for the SRO state as in this case the atomic distribution function does not extend over a long range. Again suitable atomic clusters necessarily form within these wave packets but a cluster in one wave packet is not necessarily phase related with another of the same type in a neighbouring wave packet. Intersections of wave packets with different wave vectors are possible and such superimpositions can lead to the formation of clusters with different motifs.

3.3 *Sub-unit-cell clusters*

This description envisages a random distribution of atomic clusters, which represent only parts of unit cells of the competing LRO structures. Unlike in the case of the concentration wave description, the clusters in this case do not bear any spatial relation with one another. Since these clusters do not possess all the symmetry elements of the corresponding LRO structures, the formation of these cannot be considered as nucleation of the LRO structures.

3.4 *Multiple micro-domains*

Small regions of the size of several unit cells and having structures corresponding to different competing LRO structures are visualized to coexist in the SRO state according to this description. This is plausible when different LRO structures in a given alloy are associated with nearly equal free energies. Each micro-domain can be considered to be either nearly perfectly ordered with sharp interfaces or imperfectly ordered with diffuse boundaries. The latter description, however, becomes essentially similar to the wave packet description. A variation in this description can be introduced by considering encroachment of one micro-domain over another, which results in a structure where many of the micro-domains overlap with their neighbours.

3.5 *Identical micro-domains*

This description is appropriate when all microdomains possess the same LRO structure. These micro-domains can be distributed either contiguously or in a disordered matrix. When these micro-domains are considered to be partially ordered and bounded by diffuse interfaces, the description approaches that of wave packets.

4. Summary of experimental observations

The large volume of experimental data on the nature of the SRO state and of the mode of transition from the SRO to the LRO state are summarized in this section indicating the points of concurrence and of difference between different research groups on these issues.

4.1 *Nature of SRO*

(a) On quenching from the completely disordered state Ni–Mo alloys (8–33 at.% Mo) exhibit maxima of diffraction intensity at all equivalent {1 1/2 0} positions and complete extinction at {2 1 0} positions of the reciprocal space (figure 2a). There is complete agreement between different research groups over this observation. However, interpretations offered by different groups for these diffraction effects are not the same.

As {1 1/2 0} spots can be indexed as {1 0 1} DO_{22} reflections, Okamoto & Thomas (1971) have suggested that the SRO state possibly consists of micro-domains having the DO_{22} structure. In order to account for the extinction of {2 1 0} reflections they have proposed the presence of non-conservative antiphase boundaries periodically placed along {4 2 0} planes.

The observed diffraction effect can also be rationalized on the basis of de Fontaine's (1975) concentration wave model. The fact that the calculated amplification rate as a function of the wave vector shows a maximum at ⟨1 1/2 0⟩ and a negative value at ⟨2 1 0⟩ elegantly explains why intensity maxima appears in the former position while complete extinction occurs at the latter.

(b) Dark field micrographs taken with {1 1/2 0} reflections show fine dots or a speckle contrast, the size and sharpness of the speckles increasing with decreasing quenching rate. There has been a long debate in literature whether the bright dots or speckles observed in {1 1/2 0} dark field images truly represent regions with high degree of order, which can be described as nearly perfectly ordered micro-domains. Chevalier & Stobbs (1979) have shown that in fast-quenched samples very fine speckles observed under {1 1/2 0} dark field imaging condition are not seen to be distributed within the thickness of the sample in stereo-pair-micrographs. Whereas relatively coarse dots observed in samples exposed to temperatures around 1000 K for a few seconds are found to be stereo correlatable. While the former contrast has been described as that due to the static concentration wave packet (SCMP), the latter has been attributed to micro-domains.

(c) Van Tendeloo (1976), De Ridder *et al* (1976) have proposed the presence of sub-unit-cell clusters in the SRO state of the alloys belonging to the {1 1/2 0} family. Many of the diffuse intensity features which appear during early stages of ordering can be interpreted in terms of the presence of sub-unit-cell clusters involving only a few atoms which constitute only structural elements of the competing LRO structures. The interpretation of the {1 1/2 0} reflections has essentially been based on the presence of structural units of the DO_{22} structure. The main difference between this model and the micro-domain model is in the

size of the microdomains which according to De Ridder *et al* (1976) are of sub-unit-cell dimension while Okamoto's micro-domains are made up of at least a few unit cells (Okamoto & Thomas 1971; Das *et al* 1973).

(d) Irradiation ordering experiments using 1 MeV electrons in a high voltage electron microscope have resolved the following issues. It is clear from the work of Banerjee *et al* (1984) that $\langle 1\ 1/2\ 0\rangle$ fluctuations can develop and amplify at temperatures as low as 200 K when the LRO structure is destroyed by irradiation. In fact, this observation demonstrates that the $\langle 1\ 1/2\ 0\rangle$ instability indeed exists in the system in the completely disordered state and the fluctuation amplifies as soon as kinetics of atomic migration becomes favourable. Subsequently Mayer & Urban (1985) have determined the spinodal ordering temperature for Ni_4Mo to be about 1150 ± 30 K, which is somewhat higher than T_c corresponding to the $D1_a$ ordering. The observation that SRO develops after complete destruction of LRO under irradiation of Ni_3Mo in the temperature range $200\ \text{K} < T < 450\ \text{K}$ is inconsistent with the micro-domain model of the SRO state owing to the following reasons.

(i) Micro-domains with high degree of order unlike small amplitude fluctuations cannot survive under the destructive influence of irradiation.

(ii) In a discrete process, LRO to SRO transition due to irradiation is expected to occur by the fragmentation of the LRO domains accompanied by disordering at the domain boundaries and the formation of nonconservative antiphase boundaries. Had SRO represented a state which consisted of fragmented domains of very fine size, the LRO to SRO transition due to irradiation would have occurred directly. But experiments have shown that SRO develops only from the completely disordered state and not directly in the course of disordering from the LRO state.

Irradiation experiments, therefore, suggest that the SRO state corresponds to a structure in which small amplitude short wavelength concentration waves with $\langle 1\ 1/2\ 0\rangle$ wave vectors are present. Since fluctuations with this wave vector can develop in a second order transition, the spinodal ordering mechanism becomes operative in the development of the SRO structure.

(e) Two important diffraction effects have been noted by all investigators but not much significance has been attached to these earlier. These are as below.

(i) $\{1\ 1/2\ 0\}$ reflections are quite sharp and intense and there is no significant diffuse intensity in the early stage of the formation of SRO.

(ii) All the variants of $\{1\ 1/2\ 0\}$ spots corresponding to different variants of $\langle 1\ 1/2\ 0\rangle$ wave vectors are seen in selected are diffraction patterns recorded from regions as small as $0{\cdot}2\ \mu$m in diameter.

The implications of these observations are that the $\langle 1\ 1/2\ 0\rangle$ waves extend in space to a sufficient extent to make the $\{1\ 1/2\ 0\}$ reflections sharp, at the same time, the dimensions of the region corresponding to a single wave are limited to account for the presence of all possible variants within the volume sampled in a selected area diffraction pattern.

These features are fully consistent with the concentration wave packet model (Chevalier & Stobbs 1979). In fact, this model envisages co-existence of different variants of wave vectors and their mutual overlap. It is because of this overlap of different variants and the decreasing amplitude of concentration wave at the extremetries of a given wave packet that one cannot assign sharp bounding surfaces for the wave packets.

(f) High resolution electron microscopy experiments have been carried out in order to resolve the structure of the SRO state in an atomic resolution level. High resolution images, taken by allowing the undiffracted beam and nearest eight {1 1/2 0} reflections to interfere, have shown bright dots arranged in small clusters in two-dimensional patterns representing the [0 0 1] projection of the real lattice. The bright dots were often found to be arranged in diamond-shaped or square-shaped clusters (Van Tendeloo *et al* 1985). The dimensions and the orientations of these clusters matched with the motifs corresponding to DO_{22} and $D1_a$ structures respectively. It may, however, be noted that the motifs corresponding to the DO_{22} structure and the N_2M_2 structure are remarkably similar (Kulkarni & Banerjee 1988), and therefore, are not easily distinguishable from the two-dimensional lattice resolution micrographs. However, N_2M_2 type of clusters are more likely to form in the early stages as these clusters truly represent ⟨1 1/2 0⟩ concentration waves.

Recently optical processing of such high resolution micrographs has revealed the presence of wave packets corresponding to different variants of ⟨1 1/2 0⟩ waves and their frequent interference (Lee *et al* 1988). High resolution images of SRO–LRO transitional structures, which exhibit $D1_a$ and DO_{22} motifs, show that these motifs are generated by the superimposition of wave packets associated with different variants of ⟨1 1/2 0⟩ wave vectors.

4.2 *Transition from SRO to LRO*

Evolution of the LRO structure from the SRO structure has also been studied extensively and experimental data are available for alloys with compositions centred around Ni_4Mo and Ni_3Mo and these are separately listed here.

4.2a *For Ni_4Mo alloys:*

(a) The temperature range over which the SRO–LRO transition has been studied in samples undergoing ordering in absence of irradiation is restricted to between 1000 K and 1140 K (T_c) because the kinetics of the ordering reaction below 1000 K is too slow to follow experimentally. Van Tendeloo (1976) has shown that during the early stages of ordering at 1073 K the diffracted intensity is gradually transferred from the {1 1/2 0} type spots to 1/5 {4 2 0} type spots with intensity spreading from the former to the latter positions. However, Chevalier & Stobbs (1979) have not observed such a gradual transition at 1023 K and have found the appearance of distinct 1/5 {4 2 0} spots (not linked with the {1 1/2 0} spots) to mark the beginning of the ordering reaction.

(b) Real time progress of the ordering reaction has been recorded in a much wider temperature range, 550–1020 K in an *in-situ* HVEM experinents (Banerjee *et al* 1984) where radiation enhanced diffusion expedites the ordering process. It has been reported that the SRO–LRO transition at temperatues below 800 K in a radiation environment of 5×10^{-3} dpa/s (displacement per atom per second) proceeds, at least in the initial stages, in a continuous manner characterized by the sequence of diffraction patterns as shown in figure 3. The final change noticed in the diffraction patterns is the appearance of pseudo-circles passing through the outer edge of the four {1 1/2 0} spots towards the 1/5{4 2 0} spots. It is interesting to note that from a single {1 1/2 0} spot the intensity transfers simultaneously in two directions towards (1/5){4 2 0} spots belonging to two $D1_a$ variants. Distinct (1/5){4 2 0} spots subsequently get separated from the decaying {1 1/2 0} spots at a stage when (1/5){4 2 0} dark field images show a distribution of small $D1_a$ particles in the

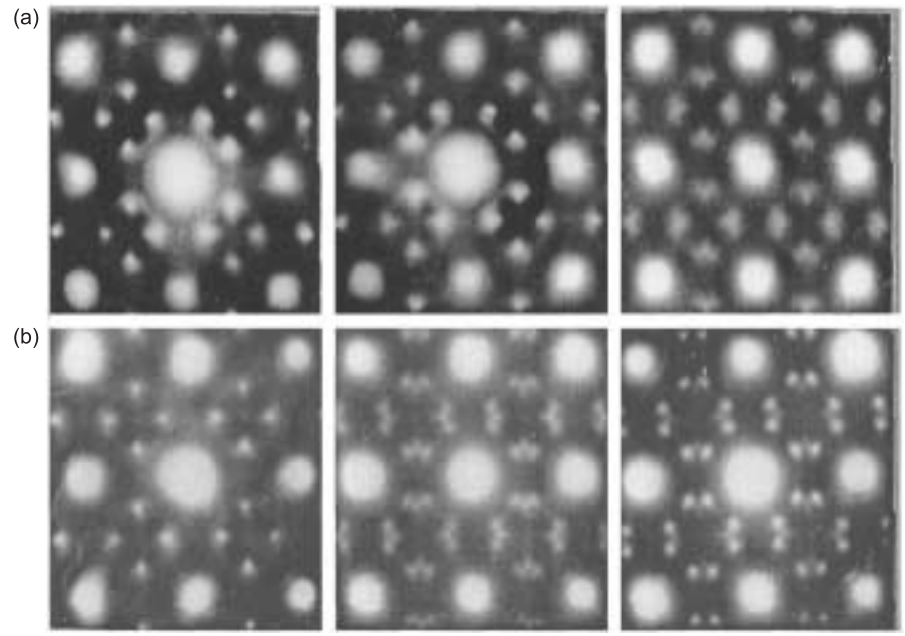

Figure 3. Sequence of diffraction patterns showing gradual changes in the Ni-20 at% Mo alloy from the SRO to the LRO state. **(a)** 573 K and **(b)** 773 K. The duration and the temperature of irradiation at a dose rate of 5×10^{-3} dpa/s are indicated. t_o represents the time ($\sim 5s$) elapsed for taking the first exposure.

matrix. The sequence of diffraction patterns observed in thermally ordered smaples by Van Tendeloo (1976) is essentially the same as that described here.

At temperatures between 800 and 1020 K under irradiation, such continuous transition from the SRO to the LRO structure has not been observed. Instead, the nucleation of $D1_a$ particles and the appearance of distinct $(1/5)\{4\ 2\ 0\}$ spots have been observed right at the beginning of the SRO–LRO transition.

4.2b *For Ni_3Mo based alloys:*

(a) In thermally ordered samples, formation of diffuse intensity passing through the four $\{1\ 1/2\ 0\}$ spots in the [0 0 1] zone marks the beginning of the transition from the SRO to the LRO structure. With the progress of this transition, maxima appear on the circle at positions of Ni_2Mo superlattice reflections. Subsequently, intensities at Ni_4Mo superlattice positions appear. Initially, intensities at the Ni_2Mo positions, remain linked but at a later stage these spots become distinct. Such a sequence of changes in the diffraction pattern can be followed when the SRO to LRO transition is induced at temperatures below about 1023 K, whereas at higher temperatures such sequential changes are skipped.
(b) The appearance of distinct Ni_2Mo superlattice relations is accompanied by the emergence of Ni_2Mo and Ni_4Mo microdomains, the former being ellipsoidal and the latter equiaxed in shape.

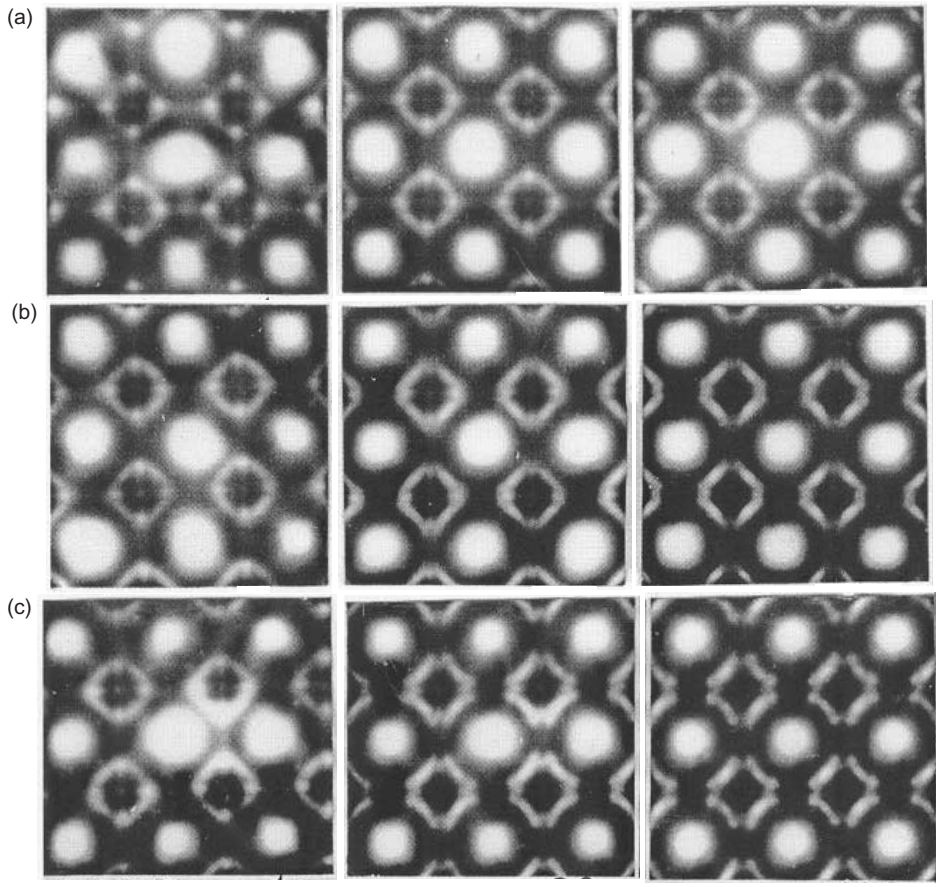

Figure 4. Sequence of diffraction patterns [0 0 1] zone axis showing the progressive changes in the diffuse intensity distribution as the Ni-25 at%. Mo alloy undergoes radiation-induced ordering at different temperatures: **(a)** 495, **(b)** 695, and **(c)** 745 K.

(c) Recent radiation-ordering experiments have probed the ordering process in a wider temperature range. This has enabled us to study the successive stages through which the system progresses during the initial stages of ordering (Banerjee *et al* 1989). The progressive changes in diffraction patterns during ordering at different temperatues are shown in figures 4 for the [0 0 1] and the [1 1 2] zone axes. The most notable feature of the SRO–LRO transition is the gradual change in the diffuse intensity distribution which links the "superlattice reflections" corresponding to different competing structures like Ni_2Mo, $D1_a$, DO_{22}, N_2M_2. The intensity of diffraction spots corresponding to different "superlattice positions" measured from the sequence of diffraction patterns has provided a quantitative description of the progress of the ordering process.

(d) Dark field images taken with the $(1/3)\{4\ 2\ 0\}$ and $(1/5)\{4\ 2\ 0\}$ reflections taken from samples in different stages of order development during irradiation ordering have shown that no resolvable micro-domains can be imaged as long as the diffuse intensity at $(1/3)\{4\ 2\ 0\}$, $(1/5)\{4\ 2\ 0\}$ and $\{1\ 1/2\ 0\}$ remains linked. Delinking of these superlat-

tice reflections marks the appearance of resolvable micro-domains of $Ni_2Mo(Pt_2Mo)$ and $Ni_3Mo(D1_a)$. The former shows an elipsoidal morphology while the latter is essentially equiaxed. In the stoichiometric Ni_4Mo alloy, the appearance of resolvable micro-domains of Ni_2Mo occurs earlier that that of Ni_4Mo. However, this sequence has been found to be the reverse in an alloy of composition closer to Ni_4Mo (Ni-22 at.%) Mo (Banerjee *et al* 1989).

(e) The association of diffraction spots in patterns corresponding to the SRO–LRO transitional states reveals that any given variant of the LRO structure (either Ni_2Mo or Ni_4Mo) evolves from SRO maxima associated with both (and not any one of) the $\langle 1\ 1/2\ 0\rangle$ wave vectors. At the same time, each one of the SRO wave vectors participates in the formation of both the variants of the Ni_2Mo and the Ni_4Mo structures. This suggests that the SRO to LRO transition involves some kind of a "co-operative interaction" of two mutually perpendicular $\langle 1\ 1/2\ 0\rangle$ wave vectors.

(f) The information obtained in the reciprocal space regarding the SRO–LRO transition has been translated into real-space information using two different approaches. Van Tendeloo *et al* (1985) have obtained high resolution images corresponding to transitional states in order to locate clusters representing motifs of competing LRO structures. This technique suffers from the drawback of the overlap of several atomic layers (typically of the order of 10–15 unit cells), which results in the partial cancellation of contrast unless the cluster extends in the direction of the electron beam. In an alternative approach simulated diffraction patterns have been generated from two-dimensional arrays of dots arranged to represent different combinations of clusters and such diffraction patterns have been compared with experimental patterns (Van Tendeloo *et al* 1985; Kulkarni & Banerjee 1988; Banerjee *et al* 1989). This simulation method has the weakness of over-simplification due to diffraction from a two-dimensional array. In spite of these shortcomings, it is clear from these studies that the SRO–LRO transitional states indeed consists of clusters of one to several 'molecules' in size, having geometries derived from the motifs representing the coherent LRO structures. The comparison of experimental and computed diffraction patterns, shown in figure 5 illustrates this point. The ingredients of cluster configurations used in generating the computed diffraction patterns are listed in table 1.

(g) In ternary alloys substitution of Mo by Al and to a lesser extent by Ta causes the normally metastable DO_{22} structure to appear and persist for a longer duration along with Ni_2Mo and Ni_4Mo during the progress of the ordering process. Addition of V or W suppresses the formation of the DO_{22} structure (Martin & Williams 1984).

5. Discussion

We shall now examine whether all the evidence collected on the ordering of Ni–Mo alloys during the last two decades and the theoretical development in this field leads to a coherent description of the ordering process in Ni–Mo alloys. There have been a number of debates in the literature on the controversies regarding (a) the nature of the SRO state, and (b) the mechanism of the SRO–LRO transition.

In view of the revival of interest in this area in the recent past it is worthwhile to examine whether there is any real controversy or there is complimentarity between different the view points.

The first question we shall address to is on the nature of the SRO structure in Ni–Mo and several other (1 1/2 0) alloys. The fact that these alloys, in the completely disordered state (i.e.

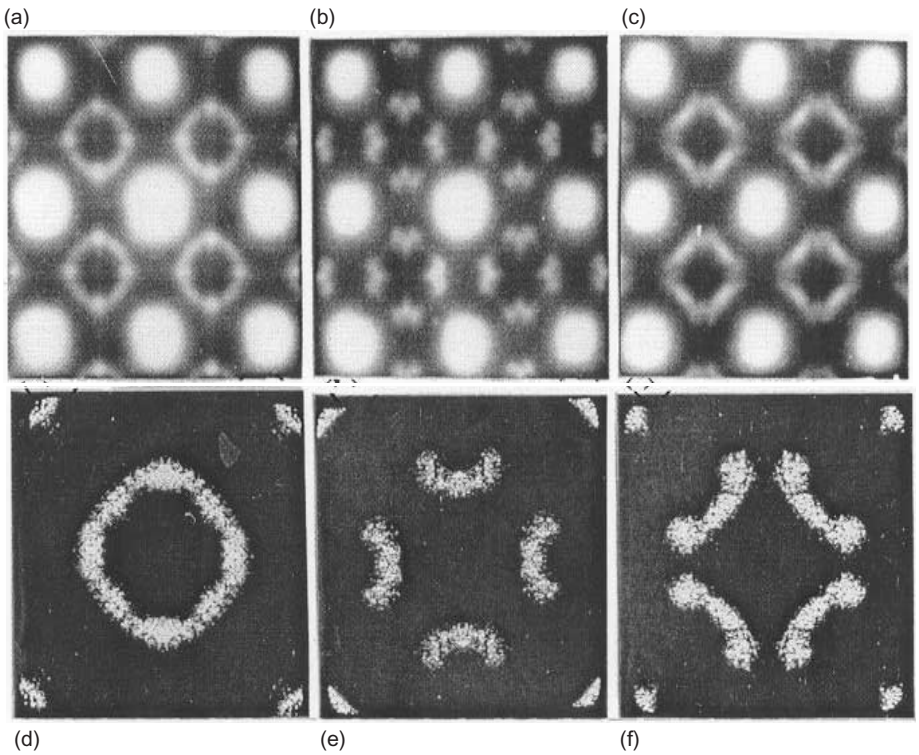

Figure 5. A comparison of experimentally observed **(a)–(c)** and computed **(d)–(f)** diffraction patterns. Different types of clusters and their sizes used for modeling the SRO–LRO transitional states are indicated in table 1.

$\eta = 0$), becomes unstable with respect to the development of $\langle 1\ 1/2\ 0\rangle$ concentration waves is now well-established both from theoretical considerations and experimental evidence. The corresponding instability temperature (T_o the ordering spinodal), has been measured for the Ni_4Mo alloy and has been found to be somewhat higher than the T_c corresponding to the first order $fcc \rightarrow D1_a$ ordering transition. At $\eta = 0$ the ordering tendency which is dictated by the magnitude of $\partial^2 G/\partial\eta^2$ selects the $\langle 1\ 1/2\ 0\rangle$ wave order as this is associated with the largest negative value of $\partial^2 G/\partial\eta^2$ amongst all the competing wave vectors. The ordering free energy of Ni_4Mo, calculated from first principle electronic structure (Arya *et al* 2001) has shown that

Table 1. Details of cluster combinations used in the generation of computed diffraction patterns in figure 5.

Computed diffraction pattern	Clusters used in simulation. Figures in brackets indicate size in number of molecules	Ratio
D	$N_2M_2(16)$, $Pt_2Mo(16)$, $Pt_2Mo(4)$	1: 1: 4
E	$N_2M_2(16)$, $D1_a(16)$, $D1_a(4)$	1: 1: 4
F	$D1_a(16)$, $Pt_2Mo(16)$, $D1_a(4)$, $Pt_2Mo(4)$	1: 2: 2: 4

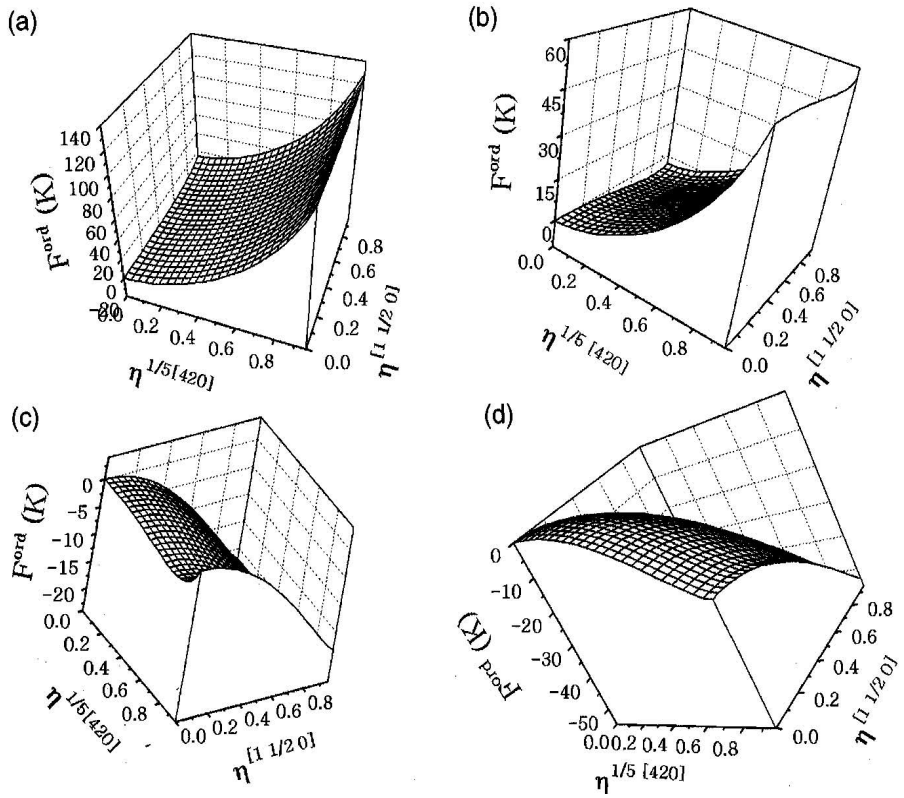

Figure 6. The ordering free energy of the Ni_4Mo-based alloy, exhibiting the $\langle 1\ 1/2\ 0\rangle$ and $(1/2)\langle 4\ 2\ 0\rangle$ ordering tendencies, plotted as a function of order parameters for the corresponding ordering wave vector at four different temperatures, **(a)** to **(d)** in decreasing temperature sequence.

the following distinct situations arise at different temperatures as far as competition between ordering reactions with $\langle 1\ 1/2\ 0\rangle$ and $(1/5)\langle 4\ 2\ 0\rangle$ wave vectors are concerned; figures 6a–d illustrate these situations.

(a) Positive curvatures for both $\langle 1\ 1/2\ 0\rangle$ and $(1/5)\langle 4\ 2\ 0\rangle$ ordering, implying stability of the disordered state (figure 6a).
(b) Negative curvature for $\langle 1\ 1/2\ 0\rangle$ and positive curvature for $(1/5)\langle 4\ 2\ 0\rangle$, implying instability of the system for $\langle 1\ 1/2\ 0\rangle$ ordering, and no ordering tendency along $(1/5)\langle 4\ 2\ 0\rangle$ (figure 6b).
(c) Negative curvature for $\langle 1\ 1/2\ 0\rangle$ and positive for $(1/5)\langle 4\ 2\ 0\rangle$ at $\eta = 0{\cdot}8$, but a dip in the free energy plot with respect to $(1/5)\langle 4\ 2\ 0\rangle$ near $\eta = 0{\cdot}8$. This implies that the system experiences simultaneous ordering tendencies towards $\langle 1\ 1/2\ 0\rangle$ ordering (second order) and $(1/5)\langle 4\ 2\ 0\rangle$ 9 (first order) (figire 6c).
(d) Negative curvature along both $\langle 1\ 1/2\ 0\rangle$ and $(1/5)\langle 4\ 2\ 0\rangle$, i.e. system experiences instabilities for $\langle 1\ 1/2\ 0\rangle$ and $(1/5)\langle 4\ 2\ 0\rangle$ ordering simultaneously (figure 6d).

The discrepancy over the variation in the size, the contrast and the stereo correlation of speckles observed in the as-quenched alloys studied by different investigators can be attributed

to the variation in the quenching rate. It is clear that 'the SRO state' is not a unique state unless the degree of order present is indicated. Depending on the quenching rate employed, samples examined by different investigators appear to correspond to different stages of the development of $\langle 1\ 1/2\ 0\rangle$ concentration wave.

All the evidence points to the fact that in the earliest stages of the development of SRO the spatial extension of each wave is sufficiently large to make the $\{1\ 1/2\ 0\}$ reflections sharp. Presence of all variants of $\{1\ 1/2\ 0\}$ reflections in the selected area diffraction pattern suggests the operation of all the variants within the smallest region ($0{\cdot}2\ \mu$m in diameter) that can be sampled. The model invoking $\langle 1\ 1/2\ 0\rangle$ concentration fluctuation is most appropriate for describing this structure.

The further amplification of such concentration waves appears to be accompanied by a localization of the fluctuations and by an interference of different wave variants. The former is evidenced in the speckle contrast, which cannot be correlated in stereo-pair micrographs. The latter process results in the generation of different motifs (or clusters) corresponding to competing coherent structures. As these clusters are generally not in phase with a single concentration wave, the SRO structure in this stage can be better described by a random distribution of clusters.

Out of the different competing wave vectors in this system both $\langle 1\ 1/2\ 0\rangle$ and $\langle 1\ 0\ 0\rangle$ vectors satisfy symmetry rules for second order transitions. Depending on the energies associated with different near neighbour interactions as discussed by Kulkarni & Banerjee (1988), fluctuations of either or both types can develop in a continuous manner. The combination of two mutually perpendicular $\langle 1\ 1/2\ 0\rangle$ waves results in the formation of Ni_2Mo and Ni_4Mo motifs while that of an $\langle 1\ 1/2\ 0\rangle$ and an $\langle 1\ 0\ 0\rangle$ waves leads to the DO_{22} motifs. It may be noted that the appearance of Ni_2Mo, Ni_4Mo or DO_{22} motifs which can independently form by the amplification of $(1/3)\langle 4\ 2\ 0\rangle$, $(1/5)\langle 4\ 2\ 0\rangle$ or $(1/4)\langle 4\ 2\ 0\rangle$ waves respectively does not necessarily require the operation of any of these wave vectors which do not qualify for second order transitions (de Fontaine 1975). Unimolecular clusters of these LRO structures can be generated by combinations of special point wave vectors like $\langle 1\ 1/2\ 0\rangle$ and $\langle 1\ 0\ 0\rangle$. This stage of order formation marks the beginning of wave coupling giving rise to an anharmonic term in the Landau expansion of the free energy expression.

There has been a long controversy over the question whether the transition from SRO to LRO occurs through a continous transition or by a nucleation and growth process. The controversy has been resolved by HVEM experiments, which facilitated the study of the SRO to LRO transition over a wide temperature range. Results of these experiments have shown that there is no unique mechanism, which is operative for the entire range of temperatures and order parameters. Different mechanisms of ordering operative in Ni_4Mo have been represented in an ordering mechanism map (Banerjee *et al* 1984).

The evolution of ordering in Ni_3Mo based alloys is still more complex because of the formation of many competing structures. Again irradiation ordering experiments have brought out the variety of evolutionary paths in which the SRO to LRO transition occurs at different temperatures under a given displacement rate. These observations have been summarized in a flow chart representation (Banerjee *et al* 1989).

The ordering mechanism map for Ni_4Mo and the flow chart depicting steps in the ordering of Ni_3Mo essentially illustrate that the experimental evidence collected on the ordering process of these alloys are not conflicting with each other. All the structural descriptions proposed indeed remain valid at least for some stages in the evolutionary path of ordering. In fact, descriptions like concentration wave and clusters have been shown to be two different descriptions of the same physical reality and the subtle differences between them are discussed in some recent

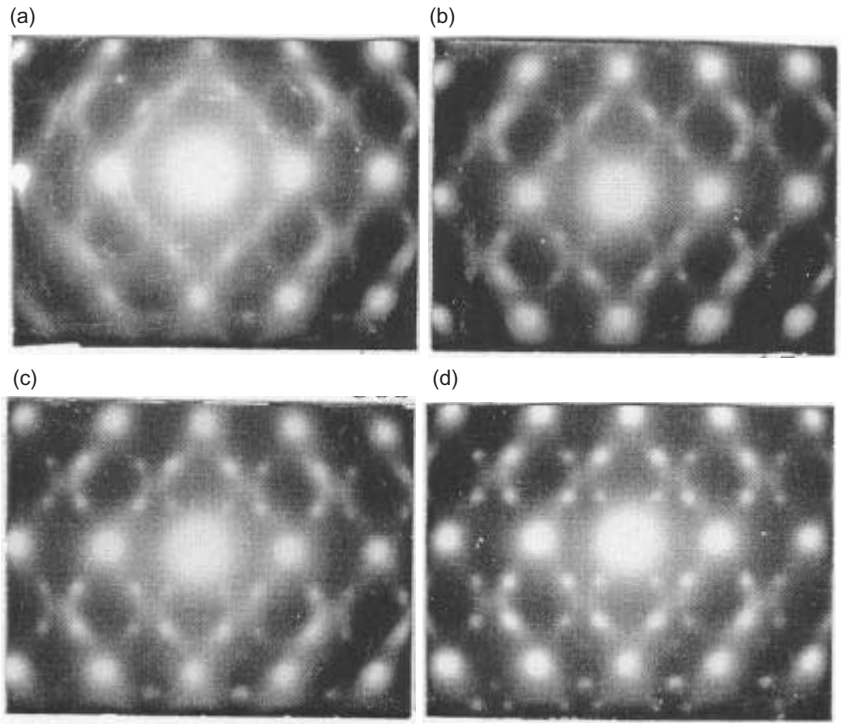

Figure 7. Progressive increase in the w reflection with irradiation time in Zr–2·5 wt% Nb alloy. Temperature = 425 K; time = 0 **(a)**, 15 **(b)**, 60 **(c)** and 300s **(d)**.

papers (Kulkarni & Banerjee 1988; Banerjee *et al* 1989). The structural descriptions, which have resulted primarily from TEM investigations, have also been found to be consistent with thermodynamic analysis.

The present paper summarizes the results obtained on replacive ordering in the Ni–Mo system under electron irradiation in an HVEM. The importance of these results in resolving some of the outstanding issues has been dealt with. A change from electron to cascade forming self ion Ni^+ irradiation was found to bring about significant changes in the stability regimes of different ordered states (Sundararaman *et al* 1995). The temperature range over which the CDO and the SRO structures persist are much wider for Ni^+ ion irradiation than for electron irradiation. The stability regime of LRO structure shrinks for self ion irradiation compared to electron irradiation. The co-existence of SRO and LRO states is not observed at any temperatures in the self ion irradiated material. Steady state structures in self ion irradiated samples are independent of the initial state of order. These observations regarding the temperature range of stability of different states for electron and self ion irradiation cases have been explained on the basis of stochastic treatments put forward by Bellon & Martin (1998) and Martin *et al* (1993) which take into account cascade size and density effects and also coherence length of the ordered structures.

Work on the influence of electron irradiation on displacement ordering is rather scarce. Figure 7 illustrates real time evolution of the ω structure during 1 MeV electron irradiation of the Zr–20 Nb alloy in an HVEM. The progressive development of sharp ω-reflections from diffuse intensities is remarkably similar to what has been observed earlier on progres-

sive lowering of the temperature in the absence of irradiation in the vicinity of the ω-start temperature. HVEM results indicate that the lattice collapse mechanism responsible for the $\beta \rightarrow \omega$ transformation under isothermal ageing is operative for electron irradiation as well.

The present review is mainly based on author's collaborative research with Prof K Urban, Drs U D Kulkarni, Dr G K Dey, Dr M Sundararaman, Dr A Arya and Prof H Wallenberger. The author is grateful to them for many helpful discussions.

References*

Arya A, Banerjee S, Das G P, Dasgupta I, Saha-Dasgupta T, Mookerjee A 2001 *Acta Metall.* 49: 3575
Banerjee S 1989 *Phase Transformations* 16/17: 389
Banerjee S, Urban K, Wilkens M 1984 *Acta Metall.* 32: 299
Banerjee S, Kulkarni U D, Urban K 1989 *Acta Metall.* 37: 35
Bellon P, Martin G 1998 *Phys. Rev.* B23 3322
Chevalier J P, Stobbs W M 1979 *Acta Metall.* 27: 1197
Das S K, Thomas G 1974a *Order–disorder transformations in alloys* (ed.) H P Warlincont (Berlin: Springer) p. 332
Das S K, Thomas G 1974b *Phys. Stat. Sol.* A21: 177
Das S K, Okamoto P R, Fisher P M J, Thomas G 1973 *Acta Metall.* 121: 913
De Fontaine D 1975 *Acta Metall.* 23: 553
De Ridder R, Van Tendeloo, Amelinckx S 1976 *Acta Crystallogr.* A32: 216
Hata S, Matsumura S, Kuwano N, Oki K 1998 *Acta Mater.* 46: 881
Kulkarni U D, Banerjee S 1988 *Acta Metall.* 36: 413
Lee K H, Hiroga K, Shindo D, Hirabayashi M 1988 *Acta Metall.* 36: 641
Martin G, Poisson F, Bellon P 1993 *J. Nucl. Mater.* 205: 301
Martin P L, Williams J C 1984 32: 1681, 1694
Mayer J, Urban K 1985 *Acta Metall.* 33: 539
Okamoto P R, Thomas G 1971 *Acta Metall.* 19: 825
Penisson J M, Bourret A 1975 *Microscopic Electronique a Haute Tension* (Paris: SFEM) p. 205
Russell K C 1984 *Progr. Mater. Sci.* 28: 229
Schulson E M 1979 *J. Nucl. Mater.* 83: 239
Sundararaman M, Banerjee S, Wollenberger H 1995 *Acta Metall.* 43: 107
Van Tendeloo G 1976 *Mater. Sci. Eng.* 26: 209
Van Tendeloo G, Amelickx S, de Fontaine D 1985 *Acta Crystallogr.* B41: 281

*References in this list are not in journal format